Simulating the GB power system frequency during underfrequency events 2018-19

Christian Cooke
School of Mathematics & Statistics
The Open University
Milton Keynes MK7 6AA, United Kingdom
christian.cooke@open.ac.uk

***Abstract*—Lightning hit a transmission powerline outside London, England on 9 August 2019. There followed a loss of power from a cascade of generator outages that exceeded contingency reserves, leading to an exceptional fall in grid frequency causing widespread transport disruptions and the disconnection of over 1m households. Simulating such events typically involves a system of differential equations representing the overall generation and load present at the time. The standard model based on the swing equation assumes unlimited capacity in aggregated resources, as well as the availability of these services for the duration of the frequency excursion. In simulating the effect of outages on the GB Grid frequency on 2019/8/9, the effect of limiting these services to the capacity of resources engaged during the event is examined. It is shown that by taking these refinements into account the timing and extent of the frequency nadir can be successfully estimated. Insight is gained into the responses of various characteristics of the grid and how they interact with unplanned generation imbalances. Using this adapted model, further events on the GB grid are examined to validate the influence of these features. With the effectiveness of the model validated, novel mitigating measures to preserve the stability of a low-inertia grid can be evaluated.**

***Index Terms*—transient analysis, frequency response, grid stability**

ACRONYMS

DR	Demand Response.
ESO	National Grid Electricity System Operator.
FR	Frequency Response.
LFDD	Low Frequency Demand Disconnection.
PFR	Primary Frequency Response.
RoCoF	Rate of Change of Frequency.
SFR	Secondary Frequency Response.

I. INTRODUCTION

The largest outage on the Great British (GB) grid in recent years occurred on Friday August 9, 2019. Lightning struck an overhead power line between Eaton Socon and Wymondley at 16:52.33 BST [8]. Two major generation units went offline almost immediately, followed by a cascade of outages that led to a cumulative power loss of over $1900\,\mathrm{MW}$. This exceeded the capacity of the reserves held to maintain the integrity of supply. As a result, the power frequency, normally $50\,\mathrm{Hz}$, dropped to $48.8\,\mathrm{Hz}$ for the first time in over a decade. This triggered exceptional measures intended to preserve the stability of the overall network. 1.15m households were disconnected, thousands of commuters were turned away from train stations, while hospitals and airports also suffered disruptions. It took 5 minutes for the frequency to recover to normal levels, and 45 minutes for all connections to be restored.

This project has received funding from the European Union's Horizon 2020 research and innovation programme under the Marie Skłodowska-Curie grant agreement No 801604.

The event on 9 August 2019 (hereafter referred to as the 2019/8/9 event) called into question the ability of the GB grid to withstand rapid changes in frequency caused by outages and surges on the network. Conventional thermal generation has traditionally provided resistance to instability through inertia: synchronous turbines converting mechanical energy to and from electrical energy to dampen the effects of sudden drops and surges in supply.

However, the stability of the power supply on the GB grid has been evolving in recent years due to the emergence of renewables as a significant contributor to the energy mix [6]. These generation sources add to the power capacity of the network but not significantly to inertia, leading to a decrease in the aggregate system inertia over time.

Whereas changes in system inertia have been shown not to affect the normal variation in frequency [15], the incidence of excursions from standard operating boundaries, including frequency events, has increased significantly in recent years [12].

This paper sets out a dynamic system to represent the principal influences on the change in frequency of the grid power supply during a transient event. It is verified first by the simulation of the 2019/8/9 event and then applied to a further 26 underfrequency events recorded by the National Grid Electricity System Operator (ESO) in the period 2018-19 [7]. Thus validated, it can be used to evaluate variations in Frequency Response (FR) services and simulate possible future mitigation measures that may smooth the transition to a stable, low-inertia grid.

Section II sets out the dynamic model used to simulate the 2019/8/9 event and the configuration of parameters necessary to recreate the state of the grid in the minutes following the lightning strike. Section III compares the output of the simulation to the frequency trace for the event, and the behaviour of the characteristics affecting its evolution in the

aftermath of the cascade of outages. Section IV applies the model to a suite of other events over the period 2018-19 to ascertain that it is generalisable, and Section V discusses the results of simulating these events using the adapted model. In Section VI conclusions are drawn from the results of the study and further avenues for research are outlined.

II. Modelling frequency response in 2019/8/9 event

Examining the frequency trace of the 2019/8/9 event (Fig. 1) the sequence can be divided into five stages, each beginning with an occurrence on the grid, as shown in the plot of the frequency data.

1) 16:52:34 Outages at Little Barford and Hornsea wind-farm follow the lightning strike, with further disconnections from loss-of-mains protections at embedded generation.
2) 16:52:58 Primary Frequency Response (PFR) halts frequency drop at 49.1 Hz, and frequency starts to recover.
3) 16:53:30 A second outage at Little Barford precipitates a further fall in frequency below 49 Hz, triggering frequency-limit disconnections in embedded generation.
4) 16:53:48 Low Frequency Demand Disconnection (LFDD) arrests the fall in frequency, which overcomes a further outage at Little Barford to recover.
5) 16:55:00 Frequency recovers to levels above the 49.5 Hz statutory threshold [10].

In this paper a model is implemented that takes into account several characteristics of the grid that would impact on the frequency. This allows us to compare their respective importance in modelling a real-world contingency.

The standard model consists of a 3-dimensional system of ordinary differential equations, based on the model detailed in [15]. This has as its foundation the standard swing equation for u, the per unit frequency deviation from the nominal (see Table III)

$$2H_{\text{SYS}}\dot{u} = p_{\text{PFR}} + p_{\text{SFR}} + p_{\text{DR}} - p_L(t) \tag{1}$$

where H_{SYS} is the inertia of the system, p_{PFR} is the Primary Frequency Response (PFR), p_{SFR} the Secondary Frequency Response (SFR) and p_{DR} is the change in demand in response to the change in frequency. $p_L(t)$ is the per unit load imbalance at time t. Each of these factors are detailed in the following sections, first describing the standard model from [15], and then setting out the changes to the model introduced to improve the agreement between the simulation and the actual frequency trace for the 2019/8/9 event.

A. Load Imbalance $p_L(t)$

From the time of the event $t = 0$ at 16:52:34, the MW imbalances $\Delta P_L(t)$ occurring up to time t are aggregated (Table I) to arrive at the total load imbalance $P_L(t)$. In (1) this is expressed as $p_L(t)$, a per unit value of the total demand at the time of the event – approximately 29 GW [8].

The example in the ESO model [9] is followed for the generation reduction at Stage 3 from 30 s–60 s after the initial outage to combine it with the second Little Barford outage. The ESO records that 350 MW of LFDD occurred at 16:53:48 [9]. This is treated as a net reduction in demand and deducted from the load imbalance from this time on.

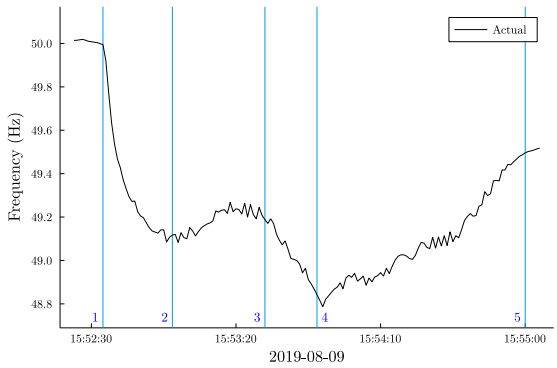

Fig. 1: 2019/8/9 event frequency trace from 1 s historic system frequency dataset provided by ESO [4]. The events marking the beginning of stages are indicated as numbered lines.

TABLE I: Load Imbalance Time Series $P_L(t)$ [9]

Stage	**Event**	t	$\Delta P_L(t)$(MW)	$P_L(t)$(MW)
1	Hornsea One	0	737	
	Loss of Mains	0	150	
	Little Barford ST1C	1	244	
	Loss of Mains	1	430	1561
3	Generation reduction	30–60	100	
	Little Barford GT1	56	210	1871
	Under Frequency Protection	66	200	2071
4	LFDD	76	−350	1721
	Little Barford GT1B	84	187	1908

B. Inertia H_{SYS}

The effect of inertia dominates in the initial seconds after the event, before Primary Frequency Response (PFR) and Secondary Frequency Response (SFR) have ramped up. At this point the standard model (1) at time $t = 1$ can be reduced to

$$\dot{u}(1) = -\frac{p_L(1)}{2H_{\text{SYS}}} \tag{2}$$

For the 2019/8/9 event $p_L(1) = \frac{1561\,\text{MW}}{29\,\text{GW}}$ and the largest per second Rate of Change of Frequency (RoCoF) from the 1 s data at the time of the event [4] is $\dot{f}(1) = 0.151\,\text{Hz}\,\text{s}^{-1}$. Given $u = (f - f_0)/f_0$, where $f_0 = 50\,\text{Hz}$, so that $\dot{u} = \dot{f}/f_0$, the result $H_{\text{SYS}} \simeq 9.1\,\text{s}$ is obtained.

C. Primary Frequency Response

PFR is intended to halt and stabilise the frequency before longer-term FR resources are ramped up (Fig. 2). The PFR value p_{PFR} is governed by the following differential equation

$$\tau_p \dot{p}_{\text{PFR}} = p_L(t) - p_{\text{PFR}} \tag{3}$$

where τ_p is the PFR time constant. The default response rate is $\tau_p = 10\,\text{s}$ (Table III). This value is the principal determinant

of the extent of the first nadir. For the 2019/8/9 event, this is adjusted to $\tau_p = 13.3\,\mathrm{s}$ to align the simulation with the event curve at this point. This could be attributed to a delay in activation that is consistent with dynamic PFR provision.

All generators connected to the GB grid must be in a position to provide PFR, including asynchronous and power-electronics interfaced resources [10]. In the model PFR is aggregated into the single variable p_{PFR}. Static PFR and Enhanced PFR are activated by the frequency crossing defined thresholds and have ramp times of $1\,\mathrm{s}$. These thresholds are crossed in the immediate aftermath of the events examined, so that these services can be adequately simulated by being aggregated into the overall PFR resrponse.

The standard PFR model assumes unlimited capacity and indefinite availability, resulting in the allocation of resources greatly in excess of those that would be feasibly available. (3) is therefore modified (4) to take into account the PFR capacity available at the time of the event (Table II), as well as a limit on the time that the full capacity of PFR resources are available.

$$\tau_p \dot{p}_{\text{PFR}} = \begin{cases} P_L(t) - p_{\text{PFR}}, & p_{\text{PFR}} < \bar{p}_{\text{PFR}} \\ 0, & p_{\text{PFR}} \geq \bar{p}_{\text{PFR}} \end{cases}$$
$$p_{\text{PFR}} = \beta_{\text{PFR}} \bar{p}_{\text{PFR}},\ t > t_{\text{PFR}} \tag{4}$$

In (4) the total capacity of PFR is $\bar{p}_{\text{PFR}}$, calculated in Table II as $922\,\mathrm{MW}$.

t_{PFR} is the time from the start of the event until dynamic, short-term PFR is disabled. The nominal value is $60\,\mathrm{s}$ (Fig 2). As with the ramp rate, this is modified heuristically so as to match the observed behaviour of the event frequency trace. In the case of the 2019/8/9 event it is set to $45\,\mathrm{s}$. β_{PFR} is the proportion of the total PFR which is static, remaining in service after dynamic PFR is terminated. The reported figure (Table II) is $\beta_{\text{PFR}} = 47\,\%$ ($435\,\mathrm{MW}$ of $922\,\mathrm{MW}$). To match the event trace, we must assume that a greater proportion of PFR remains in service after t_{PFR}, so that β_{PFR} is set to $65\,\%$.

TABLE II: PFR measures in response to 9/8 event [8]

Type	**Validated** (MW)	**Ramp time**	**Duration**
Dynamic			
- Mandatory	75% of 284	10 s	20 s
- FFR	75% of 259	10 s	20 s
Static			
- EFR	89% of 227	1 s	15 min+
- Static FFR	0% of 21	10 s	20 s
- Low frequency	71% of 31	1 s at 49.6 Hz	indefinite
- Interconnector	100% of 200	1 s at 49.6 Hz	indefinite
Total	922		

D. Secondary Frequency Response

For the standard model (1), the value for SFR, p_{SFR}, is determined by the equation

$$p_{\text{SFR}} = -K_i \theta \tag{5}$$

where K_i is the secondary control gain with default value $K_i = 0.05\,\mathrm{s}^{-1}$ (see Table III) and θ is the integral of the per-unit frequency deviation, so that $\dot{\theta} = u$.

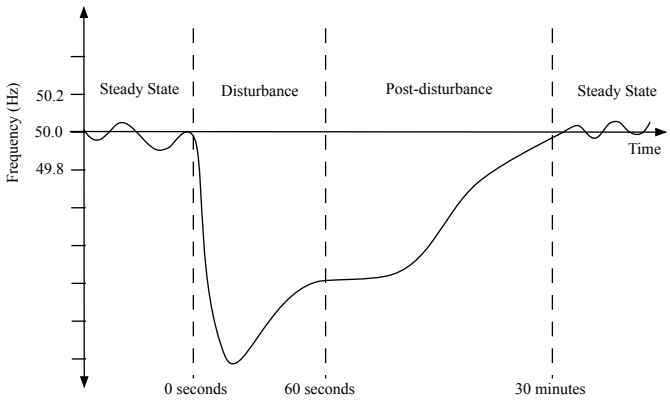

Fig. 2: Characteristic frequency trace during a system imbalance (based on [7]) showing a steady state variation within the statutory limits ($\pm 49.8\,\mathrm{Hz}$–$50.2\,\mathrm{Hz}$) followed by a sudden fall as a result of a disturbance. Recovery in frequency after the nadir plateaus after $60\,\mathrm{s}$, returning to steady state after $30\,\mathrm{min}$.

K_i is calibrated so that the slope of the recovery in frequency between Stages 2 and 3 is matched. With PFR at capacity, it is the growth in SFR at this time that alters the net imbalance on the RHS of (1). The default value of $0.05\,\mathrm{s}^{-1}$ is thereby modified to $0.013\,\mathrm{s}^{-1}$.

As the capacity of SFR is not reached over the timescale of the simulation it does not need to be accounted for.

E. Demand Response

Demand varies due to frequency, where some devices such as synchronous motors use slightly less power when frequency is low [5]. This Demand Response (DR) reduces the load from grid-connected rotating machinery. This effect is assumed to correspond to be $2.5\,\%\,\mathrm{Hz}^{-1}$ [3], so that

$$p_{\text{DR}} = 0.025\, f_0\, (u - u(0)). \tag{6}$$

As this is an effect that is not directly measurable, this assumption is the subject of debate [13].

F. Turbine Governor and Control Room Response

The generator turbine mechanical response to frequency imbalances was implemented according to [15]. With limited capacity its effects during frequency excursions were found to be reproducible through an increase in the capacity of other FR measures and it was therefore omitted from the model.

Tertiary response measures, which are activated manually, are not detailed in the event reports from the ESO. It is reported in [8] that the frequency returned to $50\,\mathrm{Hz}$ by 16:57:15 as a result of FR measures and $1240\,\mathrm{MW}$ of Control Room actions. These are reported as a result of instructions occurring after the last outage at Little Barford at 16:53:58, the last event modelled in the simulation, between Stages 4 and 5. The inclusion of these actions would see the modelled trace return to the nominal frequency more rapidly than with the support of SFR alone. Indeed the frequency after the event exceeded $50\,\mathrm{Hz}$ for a time, which may be a consequence to the Control Room interventions.

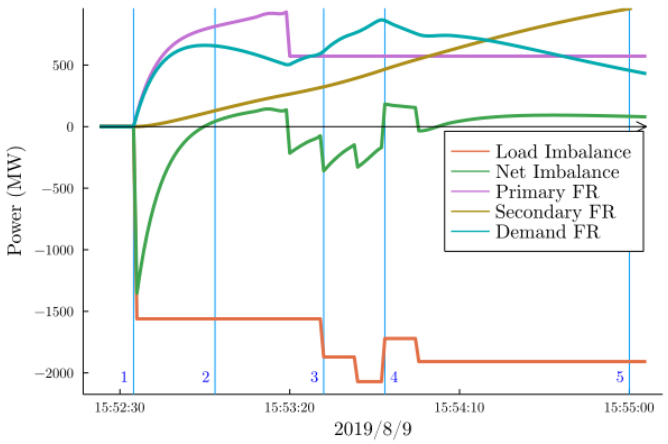

Fig. 3: Imbalance and Frequency Response graph for 2019/8/9 event.

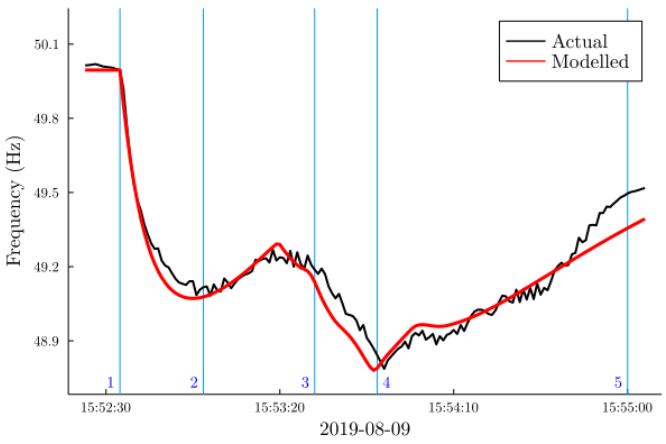

Fig. 4: Model simulation of 2019/8/9 event frequency trace.

Parameter and variable values are summarised in Table III.

TABLE III: Model Equation Values and Parameters

Parameter	Description	Unit	Default
f_0	Nominal frequency	s^{-1}	50
$f(t)$	Frequency at time t	s^{-1}	50
u	Frequency deviation $u(t) = (f(t) - f_0)/f_0$	pu	
H_{SYS}	System inertia constant	s	6
p_{PFR}	PFR	pu	
p_{SFR}	SFR	pu	
p_{DR}	DR	pu	
$P_L(t)$	Load power imbalance	pu	
K_i	Secondary control gain	s^{-1}	0.05
θ	Frequency Integral	s	
τ_p	Load reversal time	s	10
t_{PFR}	Dynamic PFRduration	s	60
α_{PFR}	DR coefficient	$\%\,Hz^{-1}$	2.5
$\bar{p}_{PFR}$	PFR total capacity	pu	
β_{PFR}	Static proportion of $\bar{p}_{PFR}$ after t_{PFR}	%	50

III. 2019/8/9 Event Model Simulation

The change in system imbalance and frequency responses during the simulation of the first 3 minutes of the 2019/8/9 event are shown in Fig 3. PFR increases to capacity $\bar{p}_{PFR}$ between Stages 2 and 3, decreasing after t_{PFR} to the level of static PFR ($\beta_{PFR}\bar{p}_{PFR}$) before Stage 3. SFR increases gradually over the 3 minutes of the simulation. DR inversely tracks changes in frequency, decreasing as it recovers. The magnitude of the DR is consistent with the expected value (c. 630 MW at 49.1 Hz [1]). The Net Imbalance is the sum of the powers on the RHS of the swing equation, (1).

The model simulation trace (Fig. 4) approximates the extent of initial nadir level (Stage 2) while being offset slightly in terms of its timing, validating the chosen value for τ_p and calculated H_{SYS}. Frequency recovers from Stage 2, the slope of recovery determined by the value for K_i setting the ramp rate for SFR. From Fig. 3 it can be seen that this is due to the net imbalance being above zero at Stage 2, until the timeout of dynamic PFR. Its decline is precipitated by the second Barford outage at Stage 3, falling rapidly as PFR capacity is reached and SFR is at too low a level to make up the deficit. Frequency is therefore in freefall. The path of the second fall in frequency is closely matched (Stage 3), as well as the timing and depth of the second nadir (Stage 4).

LFDD at Stage 4, incorporated in the $p_L(t)$ time series (Table I), returns the net imbalance to being positive, and thereafter the frequency recovers to the statutory threshold by Stage 5 as SFR increases. The initial path to recovery (Stage 5) is approximated, after which tertiary measures are reported to have intervened to correct the imbalance.

Overall the trace compares favourably with that of the ESO Frequency Simulation Engine [9].

IV. Other GB grid underfrequency events 2018-19

ESO published details of 34 over- and underfrequency events on the GB grid during the period 2018-19 [7]. Information included the magnitude and location of the disturbances causing the frequency deviation and the characteristics of the grid at the time of the event. Using the corresponding 1 s frequency data at the time of the events [11] for comparison, it is possible with this information to use the model that simulates the 2019/8/9 event and apply it to the simulation of these other events.

As the 25 underfrequency events other than that on 2019/8/9 involved a single outage, $p_L(t)$ is static, with the event occurring at $t = 0$. The loss is expressed as a proportion of the generation at the time of the event.

The time of the event is taken to be where the RoCoF is greatest, indicated by an abrupt change from normal noisy variation (Fig. 2).

One of the events in the ESO report has been omitted as having the highest proportion of inertial generation, 94.3 %, with the result that no variation in FR affects the trajectory of the frequency in the simulation, suggesting that the deficit caused by the outage was remedied by standard turbine response of the generation active at the time.

Section II-B sets out the process to calculate H_{SYS}, using the total inertial and noninertial generation at the time of the event given in the ESO report.

In calibrating the model, the PFR ramp rate, τ_p, is calibrated by matching the simulation with the frequency nadir and SFR response factor K_i is set so that the recovery path of the event trace after the nadir is matched by the simulated frequency. It was demonstrated in subsection II-D how, at this stage in the aftermath of the event, SFR is the principal determinant of the path of the frequency up to this point, once all other factors have been taken into account.

In each of the event traces there is a clearly distinguishable point where the frequency changes, usually between 30 s–60 s after the perturbation. The trajectory of the frequency alters, demarcating the boundary between different FR configurations, from which the value for t_{PFR} is taken.

The path that the frequency takes after this point is determined by the reserves available to support the recovery in frequency. With SFR set, the remaining variable is the amount of static PFR active after dynamic PFR has stopped.

In modelling these underfrequency events it is assumed that the capacity of PFR is comparable to that available at the time of the 2019/8/9 event, which is reasonable as, under the Grid Code [2], provision is to be made for PFR to mitigate the effects of an $N-1$ event, a single generator outage of 1 GW. It is also assumed that there was the same proportion of delivery at the time of these events as was the case on 2019/8/9 (Table II), taking into account the underperformance of FR providers [14], so that PFR capacity is $\bar{p}_{\text{PFR}} = 922\,\text{MW}$.

The value β_{PFR} for the proportion of total PFR that is static is determined by the behaviour of the frequency after the disconnection of dynamic PFR. With all other FR measures fixed or previously configured, the criterion that decides whether the frequency increases or decreases at this point is whether there is sufficient FR capacity to make the Net Imbalance positive or negative. This determines the sign of the RHS of (1) and thereby the increase or decrease in frequency. Varying β_{PFR} varies the amount of static PFR so that the path of the frequency can be matched.

V. 24 Underfrequency Event Simulations

In all instances of the 24 event simulations (Figs. 5, 7, 9), the initial path of the frequency after the outage matches that of the event trace, indicating an acceptable approximation of H_{SYS}.

τ_p, as measured by matching the simulation nadir with that of the event, is in the range of 4.5 s–21.5 s, apart from two instances where variations in τ_p have no effect on the nadir. These cases have the lowest loss per unit of generation at the time of the event, suggesting that normal governor response performed the role of frequency response in recovering from the shortfall.

With the exception of these cases, the total duration of dynamic PFR provision, t_{PFR} varied from 23.1 s–59.5 s (Figs. 6, 8, 10), in agreement with the standard model (Fig. 2). In

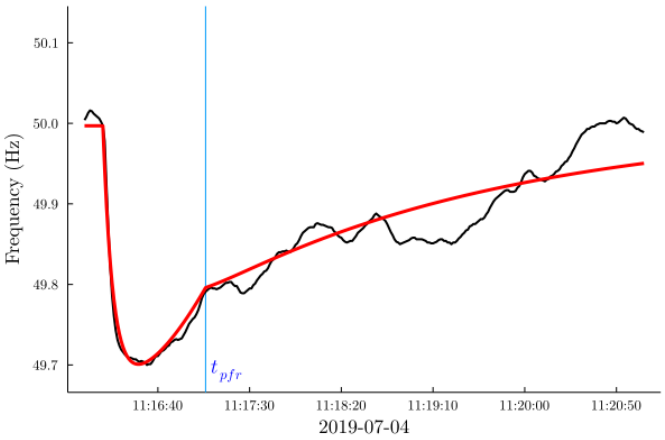

Fig. 5: Event trace for frequency event on 2019/7/4, showing a smooth recovery path.

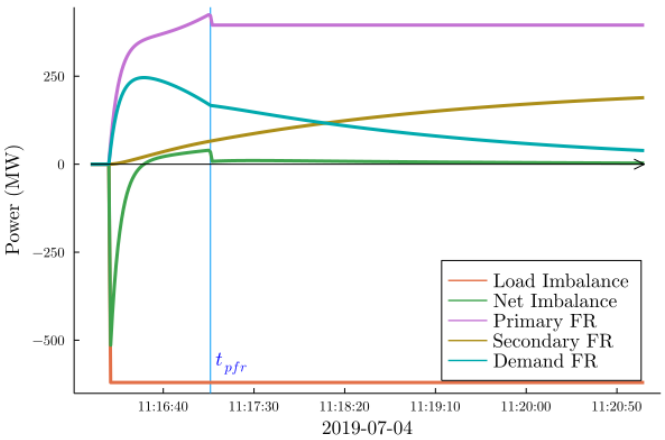

Fig. 6: Imbalance and Frequency Response graph for 2019/7/4 event. A high $\beta_{\text{PFR}} = 50\,\%$ is assumed and Net Imbalance remains positive after the initial recovery above zero.

none of the illustrated cases was the capacity of PFR, $\bar{p}_{\text{PFR}}$, reached.

In most cases, the recovery in frequency from the nadir was possible to match by calibrating K_i. From the default of $0.05\,\text{s}^{-1}$, this had a range $0.0015\,\text{s}^{-1}$–$0.06\,\text{s}^{-1}$. In the remaining cases where frequency recovers rapidly, it is possible that the origin of the outage was remedied before FR ramped up sufficiently to affect frequency.

The threshold between dynamic and static PFR outlined in Section II-C was readily identifiable in the majority of cases. From this point, three characteristic trajectories were identifiable, depending on the Net Imbalance after dynamic PFR had been disabled:

- Smooth recovery (Fig 5), where the Net Imbalance was greater than zero, so that available FR is sufficient to return frequency to stability (Fig 6).
- A kink in the frequency path (Fig 7), where the Net Imbalance dips below zero momentarily, preventing the

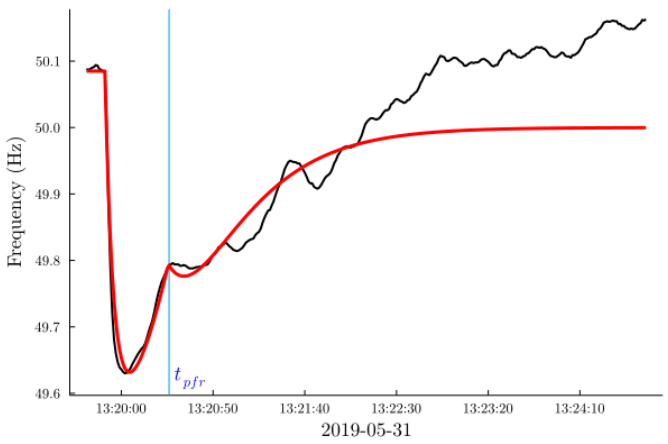

Fig. 7: Event trace for frequency event on 2019/5/31. This shows a kinked recovery path.

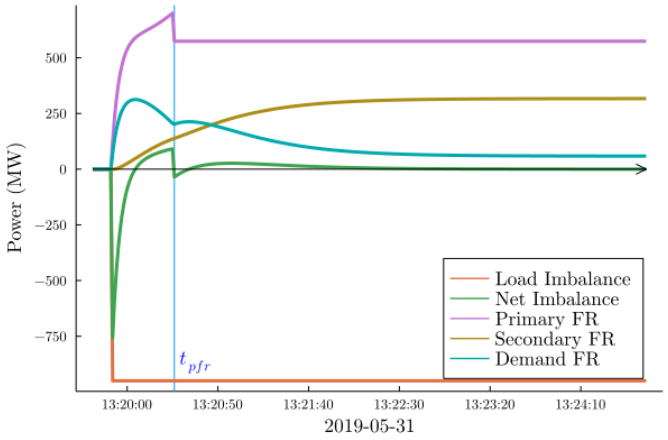

Fig. 8: Imbalance and Frequency Response graph for 2019/5/31 event. Net Imbalance is briefly negative at t_{PFR}, synchronous with the temporary drop in frequency recovery.

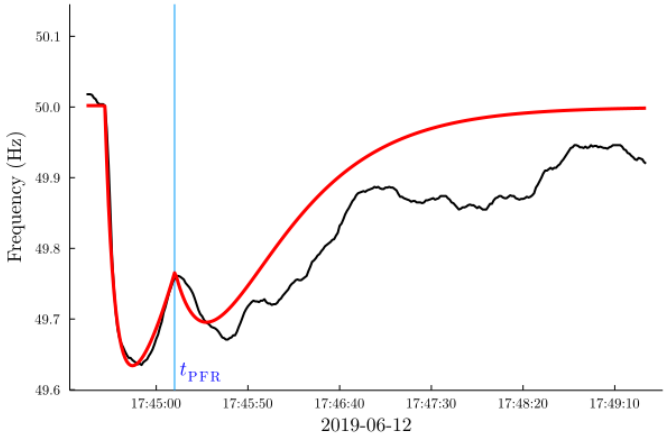

Fig. 9: Event trace for frequency event on 2019/06/12, showing a drop in frequency after the t_{PFR}, with a second nadir almost equal in magnitude to the first.

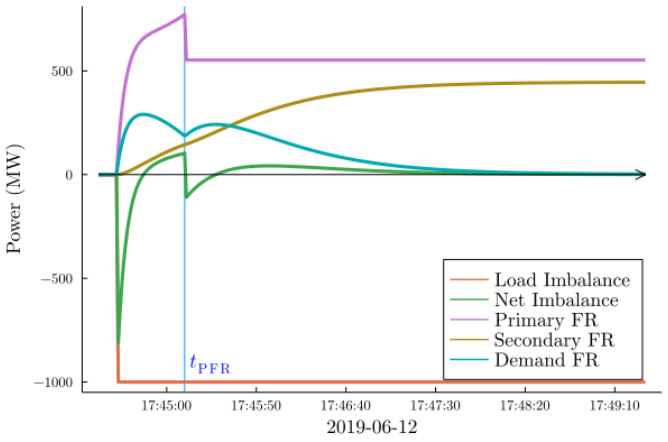

Fig. 10: Imbalance and Frequency Response graph for 2019/06/12 event. Net Imbalance is markedly negative at t_{PFR} causing the frequency to fall a second time until SFR increases sufficiently.

frequency from falling significantly, but delaying recovery until SFR increases further (Fig 8).

- A drop in frequency after the cutoff of dynamic PFR, to levels near to or exceeding the initial nadir (Fig 9), where the Net imbalance is markedly negative at t_{PFR} and FR is insufficient to stabilise the drop in frequency until SFR increases to the point where it makes the Net Imbalance positive again (Fig 10).

Matching each of these trajectories is done by the calibration of β_{PFR} to quantify the amount of static PFR available after the cutoff at t_{PFR}, and thereby the FR resources to balance the deficit. In the simulations of the 2018-19 events, this value ranged from 10 %–91 %, a significant variation in grid behaviour. Correspondence between the simulation and the event traces reduce after the dynamic PFR cutoff point. Whereas the 2019/8/9 event was well documented in reports by ESO and Ofgem (the energy regulator) [8] [9] [14], there are no details in the ESO report on frequency events on secondary outages. Such outages were a significant contributor to the magnitude of the 2019/8/9 event, and during the period 2018-19 many of the same Loss of Mains protection systems would have been in place, responding to sudden variations in voltage and frequency. It is therefore only possible to simulate the overall path of the frequency in the absence of this information.

VI. Conclusions

In this paper the behaviour of grid frequency during the 2019/8/9 event and other underfrequency events on the GB grid in the period 2018-19 is simulated. For this a 3-dimensional dynamic model which accounts for characteristics of grid FR is devised. From this work the following conclusions can be drawn:

1) Frequency transients and FR services can be adequately modelled using a dynamic system so that the behaviour

of the frequency in response to a Net Imbalance can be examined.
2) In modelling major transient events, the capacity of FR reserves must be taken into account. Once this level is reached, FR must remain static for the remainder of the simulation, or for the contracted duration if this applies.
3) The limit on the duration of the availability of dynamic PFR should be allowed for, and the proportion of total PFR available after this ends calibrated to the trajectory of frequency recovery.
4) The inclusion of DR is important for accurate transient modelling, but the basis for simulating its frequency sensitivity during excursions should be scrutinised.

While it has been shown that a reasonable approximation of an event frequency trace can be achieved using realistic parameters, and the generality of the model demonstrated by examining other underfrequency excursions on the GB grid, the model would benefit from extended analysis. Greater detail on the underfrequency events would allow a more in depth study of FR services. The effects of geographic distribution of generation, inertia, and FR should be examined, as well as testing the model on events in other grids. This will involve the adaptation of the grid configuration on these grids at the time of these events and a comparison of the results. Effects such as inertia, DR and FR are configuration dependent, and their effects on obtaining good simulation results in a variety of scenarios should be investigated.

Overfrequency events should also be examined to see how the model handles excursions above the statutory level.

Disaggregation of PFR and SFR into their static and dynamic components with varying time constants and service durations would result in a closer correspondence between the simulation and the actual grid configuration. This had been investigated in preliminary work but was found to be unnecessary for a first approximation of frequency behaviour. The contribution of deadbands and generator turbine response to the accuracy of an event trace, also not included in the model after experimentation, should be reexamined.

ACKNOWLEDGMENT

The author would like to thank his supervisor Dr. Benjamin Mestel for his enduring support and patient direction; Prof. William Nuttall, Dr. TC O'Neil and Dr. Katrine Rogers of the supervisory team for their experienced guidance; and Prof. Ettore Bompard, Dr. Carmelo Mosca, Prof. Petr Vorobev and Prof. Janusz Bialek for their valuable advice.

REFERENCES

[1] Janusz Bialek. What does the GB power outage on 9 August 2019 tell us about the current state of decarbonised power systems? *Energy Policy*, 146:111821, 2020.
[2] National Grid ESO. Operating code no. 6 (oc6) demand control. Technical report, National Grid ESO, https://www.nationalgrid.com/sites/default/files/documents/36903-OC6%20Demand%20Control.pdf, November 2014.
[3] National Grid ESO. System operability framework. Technical report, National Grid ESO, 2016.
[4] National Grid ESO. National grid eso system frequency dataset, August 2019.
[5] National Grid ESO. Interim technical report on the events of 9 august 2019. Technical report, National Grid ESO, 2020.
[6] National Grid ESO. Operating a low inertia system. Technical report, National Grid ESO, 2020.
[7] National Grid ESO. System Operability Framework – Past Frequency Events. Technical report, National Grid ESO, https://www.nationalgrideso.com/document/156761/download, 2020.
[8] National Grid ESO. Technical report on the events of 9 august 2019. Technical report, National Grid ESO, https://www.nationalgrideso.com/document/152346/download, 2020.
[9] National Grid ESO. Technical report on the events of 9 august 2019 - appendices. Technical report, National Grid ESO, 2020.
[10] National Grid ESO. Grid code (uk), 2021.
[11] National Grid ESO. System frequency data. Technical report, National Grid ESO, https://data.nationalgrideso.com/system/system-frequency-data, 2021.
[12] Samuel Homan and Solomon Brown. An analysis of frequency events in Great Britain. *Energy Reports*, 6:63–69, May 2020.
[13] Callum MacIver, Keith Bell, and Marcel Nedd. An analysis of the August 9th 2019 GB transmission system frequency incident. *Electric Power Systems Research*, 199:107444, 2021.
[14] Ofgem. 9 august 2019 power outage report. Technical report, Ofgem, 2020.
[15] Petr Vorobev, David M. Greenwood, John H. Bell, Janusz W. Bialek, Philip C. Taylor, and Konstantin Turitsyn. Deadbands, droop, and inertia impact on power system frequency distribution. *IEEE Transactions on Power Systems*, 34(4):3098–3108, July 2019.